Heat set creases in polyethylene terephthalate (PET) sheets to enable origami-based applications

IOP Publishing Smart Materials and Structures
Smart Mater. Struct. **28** (2019) 115047 (13pp) https://doi.org/10.1088/1361-665X/ab49df

Heat set creases in polyethylene terephthalate (PET) sheets to enable origami-based applications

Brandon Sargent[1], Nathan Brown[1], Brian D Jensen[1], Spencer P Magleby[1], William G Pitt[2] and Larry L Howell[1]

[1] Department of Mechanical Engineering, Brigham Young University, Provo, UT, 84602, United States of America
[2] Department of Chemical Engineering, Brigham Young University, Provo, UT, 84602, United States of America

E-mail: lhowell@byu.edu

Received 7 May 2019, revised 26 August 2019
Accepted for publication 1 October 2019
Published 24 October 2019

Abstract

Polyethylene terephthalate (PET) sheets show promise for application in origami-based engineering design. Origami-based engineering provides advantages that are not readily available in traditional engineering design methods. Several processing methods were examined to identify trends and determine the effect of processing of PET sheets on the crease properties of origami mechanisms in PET. Various annealing times, temperatures, and cooling rates were evaluated and data collected for over 1000 samples. It was determined that annealing temperature plays the largest role in crease response. An increase in the crystallinity of a PET sheet while in the folded state likely increases the force response of the crease in PET sheets. An annealing time of at least 60 min at 160 °C–180 °C with a quick cooling results in a high force response in the crease. The effectiveness of the processing methods was demonstrated in several origami patterns of various complexities.

Keywords: origami, polyethylene terephthalate, heat set, origami manufacturing, compliant mechanisms

(Some figures may appear in colour only in the online journal)

1. Introduction

Origami, the art of paper folding, has recently been investigated for use in creating mechanisms and structures for engineering applications [1–3] such as a ballistic barrier shown in figure 1(a) or a debris shield for space applications shown in figure 1(b). These origami-based mechanisms have advantages that are not readily available in traditional engineering mechanisms, including being monolithic, highly compressible and compact, and achieving all motion through compliance. Some origami patterns are easily tessellated [4–6] and some create metamaterial behavior, exhibiting interesting motion uncommon in traditional materials or mechanisms [7, 8]. Uses of origami and the parameters that define the characteristics of the various fold patterns have also been the subject of recent studies [4, 9–12]. Research in applying origami patterns to engineering and methods for actuating these mechanisms through an understanding of the material and crease behavior from which the origami mechanisms are constructed has also been actively investigated [13–24].

Although techniques have been developed to expand origami-based design beyond sheet materials [27–29], many origami-based applications use materials that are a sheet or a film with negligible thickness and yet can hold a crease. For example, Butler *et al* [26] investigated creating an origami-based mechanisms using BoPET, Tyvek®, Kapton®, UHMWPE, and ETFE sheets (Kapton® mechanism shown in figure 1(b)).

This study investigates the use of polyethylene terephthalate (PET), a common polymer often found in thin

(a) Origami-inspired ballistic barrier [25]

(b) Origami-inspired debris shield for space applications [26]

Figure 1. Origami-inspired mechanisms. (a) Origami-inspired ballistic barrier [25]. (b) Origami-inspired debris shield for space applications [26].

sheets such as in consumer liquid containers. Due to the availability of PET and favorable characteristics of the PET sheets for origami folding, it has been considered for use in origami design [21, 22, 30–32].

The usefulness of a material for origami applications often depends the properties of the creases. Important characteristics of crease behavior are the natural or unstrained position of the crease and the force response of the crease. In rigid origami mechanisms, or mechanisms made from patterns that only require strain at the crease lines, the panels can be considered as links and the creases compliant joints. As a compliant joint, the crease has a natural, lowest-energy state towards which it will return. As a sheet material is creased, it plastically deforms to a new natural position referred to here as holding a crease. Some materials, such as many consumer fabrics, do not hold a crease without some additional processing, such as ironing. Other materials, such as metals, will hold a crease, but due to limited elastic ranges, folding the material requires much more plastic deformation. Also, the act of creasing the material can cause the material at the crease to harden. This makes the crease stiffer than the surrounding panels and actuation along the same crease line more difficult. Conversely, paper has a decreased stiffness at the crease, allowing for motion around the crease axis. Some materials, such as some polymers with larger elastic regions, can be formed into a fold position and be actuated from the folded state while retaining their bias to the natural state similar to how traditional springs have a natural length. This bias can be useful for self-deployment, easily returning to a home configuration for storage, or pre-tensioning for additional stability in a mechanism. The amount a crease is biased to a given configuration can be observed by measuring the force exerted by the crease when actuated from the natural configuration.

Polymers often have larger elastic strains than metals, allowing them to undergo larger deformations and actuation at creases before yielding. A disadvantage to using polymers is their tendency to experience high stress relaxation. Stress relaxation is characterized as the reduction in force response of a material when held at a constant strain for a period of time. Understanding the stress relaxation of creases is also an important part of origami engineering design. Due to its stiffness, PET sheet is a good candidate for origami applications because it can maintain a crease and bias toward the folded state. This work investigates the effects of processing methods on the creases in PET sheet material and biasing of the material to a given folded state. Understanding the trends and parameters of the annealing process and the ability of PET sheets to be annealed to a designed position can assist in the development of future applications of polymer-based origami engineering and provide a framework for future studies.

1.1. Review of material properties

PET is a semi-crystalline thermoplastic polymer. This means that a PET sample is a combination of amorphous regions and crystalline lamellae [33]. The degree of crystallinity has a large effect on its physical properties [34]. Increases in crystallinity can increase the elastic modulus and the strength of the polymer through increased intermolecular bonding [35, 36]. Changes in crystallinity also influence optical properties. As crystal growth occurs in PET, the visible haze of the polymer increases [37]. These changes can be observed by measuring optical density. PET also has a relatively high glass transition temperature (T_g) and a slow crystallization rate. These lead to highly different physical properties based on the thermal and mechanical processing of the polymer sheet. The stresses placed on the polymer and the heating process are two of the largest contributors to the crystallinity and orientation of the molecules. Research has investigated the effect of processing on the crystallinity and crystal growth of PET sheets and fibers [33, 34, 38–40].

Amorphous PET has a cold-crystallization temperature of $T_c \approx 135\,^{\circ}\mathrm{C}$ [40]. Cold-crystallization occurs when the polymer is heated above glass transition ($T_g \approx 75\,^{\circ}\mathrm{C}$ for PET) and the molecules in the amorphous state can move sufficiently to begin organizing into crystalline structures. These materials will eventually melt as the temperature approaches the melting temperature ($T_m \approx 250\,^{\circ}\mathrm{C}$). Flores *et al* [33] studied the various levels of crystallinity of samples annealed at temperatures from 100 °C–190 °C for nine hours to induce cold-crystallization. Samples annealed at lower temperatures started with a lower crystallinity. When heated

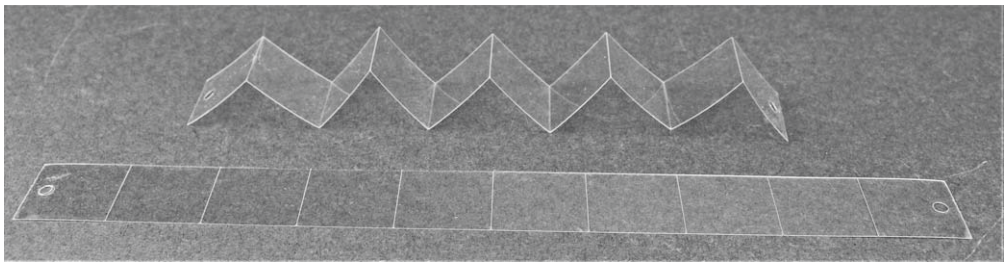

Figure 2. A scored sample before folding (bottom) and a scored and creased sample (top). The natural state of the sample after creasing and before processing is in a partially folded state. Holes used to attach to the tensile tester can be seen in the first and last panel of the sample strips.

again at 2 °C min^{-1}, all samples reduced in their level of crystallinity initially, but those annealed at a lower temperature (less than 160 °C) then increased in crystallinity when transitioning through the annealing temperature range until reaching T_m. Similar, but not as prominent trends were seen at a heating rate of 40 °C min^{-1}. They observed that the higher heating rate limited the reorganization of the internal polymer structure.

Karagiannidis *et al* [38] discovered that PET sheets can increase in crystallinity at temperatures less than the cold-crystallization temperatures. They annealed their samples at 115 °C for 0–30 min and noticed an increase of crystallinity of up to 30%. Abou-Kandil and Windle [39] focused on the formation of the microstructure of amorphous PET samples as they were drawn and then annealed. They found that when a sample is stressed in a direction, a mesophase liquid crystalline phase (smectic-A structure) is formed prior to full crystallization. They also found that the chains of the polymer arranged themselves in the direction of the draw.

Cho *et al* [34] showed that for a short heat treatment in a free-to-relax condition, PET fibers would decrease in yield stress while maintaining a high elastic modulus. This was due to the formation of micro-crystals in the heated areas. The heat treatment was for just over one second at around 190 °C. Similar results were found with rapid heating of as-spun fibers with a CO_2 laser [41].

The strain rate also plays a role in the crystallinity of the final PET product. This is due to strain-induced crystallization. Martins *et al* [40] observed that strain hardening occurs in two phases: (1) a smooth increase in stress with rapid increases in crystallinity up to 15% crystallinity and (2) a sharp increase in stress with little change in crystalline structure. For very high strain rates, the crystallization did not occur until after the strain and was greater than when strained at lower rates or at high temperatures. They concluded that slower strain rates at high strain values help improve the organization of the crystals. This also produces more uniform thickness. However, when higher crystallinity and higher orientation at the end of the process is desired, one should use faster speeds at higher strains.

This study investigates several processing methods and their effect on the force response of folded PET sheet samples with a particular focus on application to origami-based applications. The link between increasing crystallinity in a given folded configuration and the force response in that configuration is discussed. As the material properties change as a function of thermal and mechanical processing, the change of the force response is observed. An understanding of the response and possible causes of this response is important as the applications for origami engineering vary broadly.

2. Methods

To understand the force response of a crease for a given processing method, a simple fold pattern was selected for testing. Once an understanding of the important processing parameters was obtained, the effectiveness of the processing was validated in more complicated origami patterns.

2.1. Sample manufacturing

Flat sheet samples were cut from clear PET sheet from McMaster-Carr with thickness of 0.127 ± 0.012 7 mm. Using a CO_2 laser, equally-spaced fold lines were etched into sheet strips. This was done at 3% of the laser power to score the sheet without cutting it. The laser was used to ensure the accuracy and repeatability of the fold pattern and is a common method used in origami engineering to ensure precise lines in a fold pattern. To ensure that the laser scoring did not adversely effect the samples, strips of scored and unscored PET sheets were evaluated in tensile tests. The laser had little affect on the elastic modulus and yield strength of the plastic, which corresponds with previous findings for PET fibers [34, 41]. Since the use of PET in origami mechanisms typically work in the elastic region, the use of laser scoring is not expected to have an adverse effect on the final performance of the origami models. Similar pattern manufacture methods have been used previously in PET origami applications [21].

Strips of PET 254 mm by 25.4 mm were cut with lines scored every 25.4 mm along the length creating nine folds and ten panels. Holes were cut in the first and last panel for attachment to the tensile tester. A simple Z-fold was creased into each test sample. A scored sample strip and a scored and creased sample strip are shown together in figure 2. The natural state of the creased sample was in a partially folded configuration. Tensile tests were again performed on a set of randomly selected test samples to ensure that there was not a significant difference in the samples.

2.2. Processing

Samples were labeled, folded, and pressed into a fully compressed state constrained between two thin aluminum plates. Each pattern was processed in batches of ten samples using a combination of the processing variables described in table 1, resulting in 100 distinct combinations, 71 of which were tested. Preliminary testing on a wide range of times and annealing temperatures between T_g and T_m, as well as cooling methods, was conducted to narrow the range of the variables used to those in table 1. Preliminary testing showed low force responses and high relaxation when the samples were cooled rapidly through T_g. This could be attributed to the high cooling rate not allowing for the reorganization of the internal polymer structure as was similarly seen during heating [33]. Two rates of cooling were used in cooling the samples. The first, a cooling process referred to hereafter as 'Slow' cooling, was performed as the samples were allowed to cool (approximately 0.5 °C min^{-1}) in the oven back to ambient temperature T_a. In the second, referred to as 'Drop Cooling', the air temperature in the oven was quickly lowered from the anneal temperature to 90 °C (approximately 15 °C min^{-1}), and then the samples were slowly cooled from 90 °C to T_a (approximately 0.5 °C min^{-1}). This cooling method partially precludes cold-crystallization similar to quenching but allows for some reorganization by slowly passing through T_g. All possible combinations were evaluated for temperatures from 120 to 170, where temperatures above 180 were limited to primarily the Drop Cooling at 60 min. This was done due to processing difficulties (panel adhesion discussed later) and preliminary trends that suggested that temperature was the dominating factor. Therefore, the batches above 170 were reduced to primarily test for temperature change, using 60 min annealing times and Drop Cooling. A total of 1023 samples yielded usable data.

After the cooling process, the samples were removed from the plates and if there was any adhesion between the panels, a thin knife was run between the panels to separate the panels while taking care not to flex the joint. Panel adhesion occurred at higher temperatures and will be discussed in greater detail in subsequent sections. Figure 3 shows the sample labeled 649 as an example of how the z-folded sample strips appeared after processing.

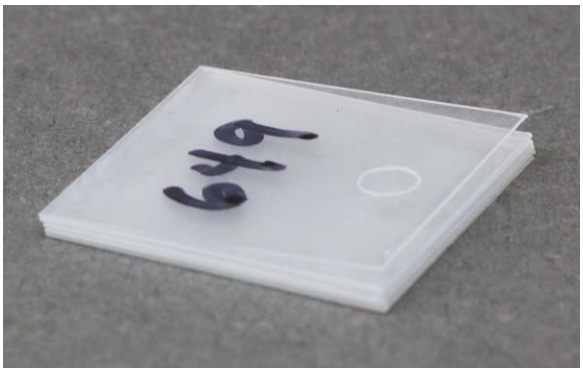

Figure 3. Sample 649 given as an example of how the z-fold sample strips appeared after processing. The samples were constrained in the fully folded position during processing but after processing, the natural state changed to the fully folded position, no longer requiring the constraints. Sample 649 was processed at 160 °C for 90 min with Drop Cooling.

Table 1. Variables used in processing methods for the sets of test samples.

Annealing time (min)	Anneal temperature (°C)	Cooling rate
60	120	Drop
75	130	Slow
90	140	
105	150	
120	160	
	170	
	180	
	190	
	200	
	210	

2.3. Testing

An Instron 3345 tensile tester was used to record force-displacement data. The Instron was set up to measure the data using an Interface SMT1-1.1 5 N load cell with an uncertainty of .04%. The Instron used had a position control resolution of 0.133 μm. Sample pulling hooks were placed on both the stationary base and on the force cell to be used to secure the ends of each sample. Once the setup was complete, the load cell was calibrated. This setup and calibration was done before every testing session, ensuring equivalent testing conditions and calibrations.

Samples were placed into the Instron setup by placing the hole of each side of the sample onto the sample pulling hooks. The initial crosshead displacement was zeroed to the largest distance at which panels 2 through 9 remained in full contact with each other. Creases 1 and 9 were slightly opened to allow the sample to be placed on the pulling hooks, however all other creases remained fully folded. After zeroing the initial displacement, the force was also zeroed. This ensures that the recorded force reflects the force due to the added displacement in each individual sample.

Using the described setup, each sample set was tested under two different loading conditions. Eight samples from a batch were individually pulled in a tensile test by displacing the cross head to 165 mm (at a average rate of 12.7 mm s^{-1}) and then returned to the initial length. Assuming 205 mm to be the maximum displacement before stretching the material panels, the reported displaced distance of 165 mm is approximately 80% of the maximum possible displacement. This was chosen to be well under the maximum displacement before stretching the material to ensure the displacement came from the unfolding of the sample. Strain in the panels and small amounts of yielding at the creases was expected. Test displacement was driven by a testing program in which the Instron crosshead would displace the desired 165 mm for each test. The force-deflection relationship was observed for both the extension and return. The maximum force response was

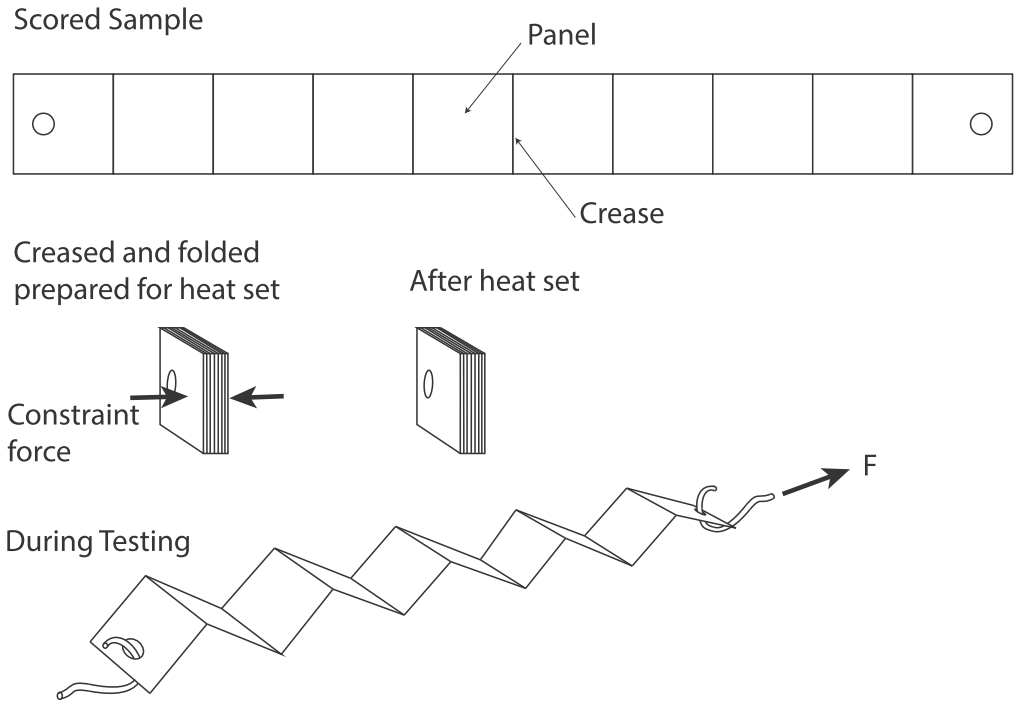

Figure 4. Schematic of testing methods.

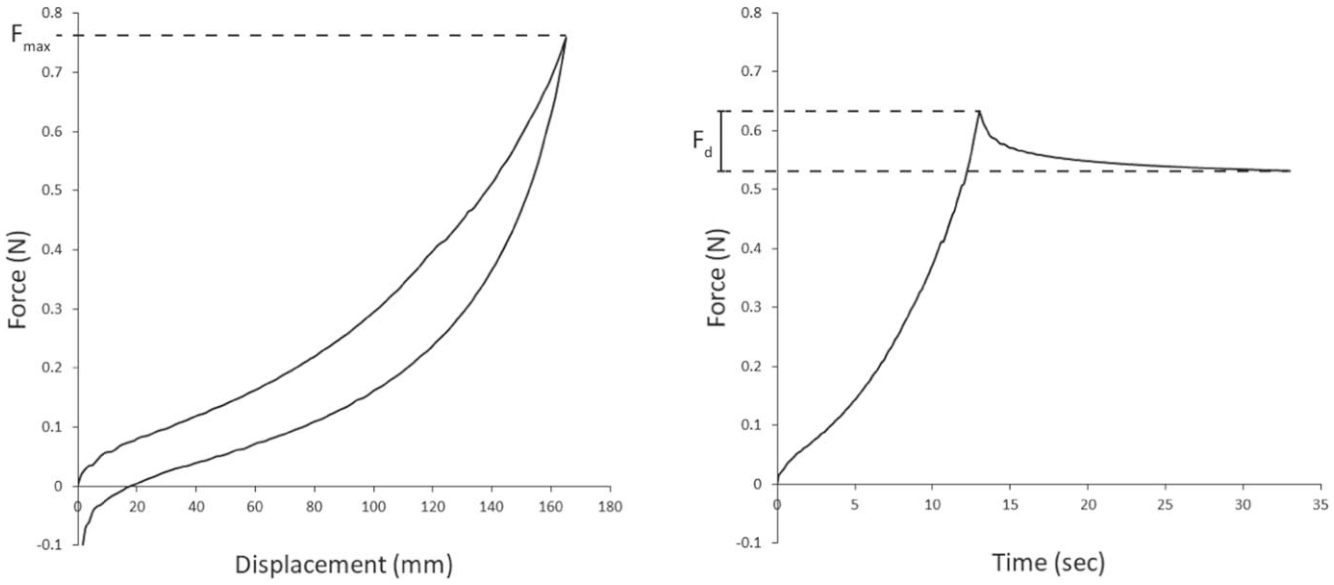

Figure 5. Typical curves obtained during testing. $F_{\max}$ obtained from sample 771 and F_d from sample 919. These samples were randomly selected.

recorded, $F_{\max}$. Between each test, the crosshead displacement and force was zeroed for each sample. This ensures that there is no drift in the observed data. In accordance with the displacement resolution of the Instron, every sample test began at the same length and was stretched to the same displacement.

The second loading condition was designed to determine the effect of stress relaxation. Two samples from a batch were individually pulled to 165 mm at the same rate as before and held for 20 s. The force-time relationship was observed. The initial maximum force exerted by the sample and the final force exerted were noted. The difference was recorded as the 'Force Drop', F_d. The Force Drop was considered to be an indication of the severity of stress relaxation for a given processing method. Figure 4 shows a schematic of the testing methods. Figure 5 shows typical curves obtained during testing obtained from two randomly selected tests. The hysteresis shown in the curve does indicate that a small amount of plastic deformation occurred during unfolding. Some small position error could be introduced through shifting of the hook in the specimen attachment hole; however the constant tension in the specimen kept the specimens steady in the

mount. Any motion due to repositioning the hook was relatively small in comparison to the measured extension.

Random samples were taken from each temperature group and a visible light scattering test was performed using a Beckman Coulter DU 640 Spectrophotometer. Each selected sample was stretched and mounted in the test apparatus such that panel 3 laid flat over the aperture. A light (wavelength $\lambda = 600$ nm) was passed through the sample and the scattering of the light was quantified as the optical density, OD, between the treated and untreated sample as described by equation (1) where $I_{untreated}$ was the intensity of light after passing through a control sample and $I_{treated}$ represents the light intensity after passing through a heat treated sample

$$\mathrm{OD} = -\log\left(\frac{I_{treated}}{I_{untreated}}\right). \quad (1)$$

2.4. Physical validation in origami patterns

Once we obtained a greater understanding of the expected response of the crease due to processing, a processing method resulting in a stiff crease was selected for validation in origami models. These models varied from simple to complex, to test the range of application of the processing methods.

The origami models chosen are:

1. The Miura-ori tessellation [21, 23, 42–46].
2. The Flasher pattern [47, 48].
3. A modified triangulated cylinder tessellation [49].
4. The elliptic infinity pattern [50, 51].

3. Results

As the temperatures increased above 170 °C, adhesion became increasingly pervasive in the panels. Slight adhesion was observed at the cut edge (where the laser cut the sample from the main polymer sheet) at all temperatures, but at anneal temperatures above 170 °C, significant adhesion in the panel faces themselves began to be observed. Above 190 °C the adhesion became so severe that some samples were untestable as they had completely adhered or failed while attempting to separate the panels. Small sheets of aluminum foil were inserted between the layers to prevent adhesion. This proved an effective way to solve the adhesion problem, but the change in processing method prevents these samples from being directly compared to the rest of the data.

As processing and testing continued, the spread in resulting data from each batch began to decrease. A second round of tests was performed using the same conditions as the first 50 batches on new samples. These repeated batches maintained a similar average and trend as the first 50 batches with a tighter distribution.

A statistical analysis was performed on the data collected with and without including the self-adherent samples above 190 °C and with and without the first 50 batches (where personnel experience could have played a factor in the results). All variables were considered with their interactions to create all possible models to fit the data using multiple linear regression models. A minimum BIC criteria was used to determine the best model for each case. Some outlier samples were removed prior to analysis due to physical conditions that made the data for the test unusable. The most common of these was adhesion in the panels that increased the force to unfold as it was separating the adhesion and not unfolding the sample. Case-Influence statistics such as studentized residuals and Cook's distance were calculated to ensure that no serious outliers in the usable data were affecting the models.

The results from the statistical analysis for $F_{\max}$ versus all possible statistical models and F_d versus all possible statistical models resulted in the same explanatory variables, temperature and temperature squared. This indicates that the other variables (annealing time and cooling rate) and their interactions cause little statistical significance on the force and stress relaxation response of the creased sheet.

When the first 50 batches with higher spread were removed and only the repeated samples were examined, the results were the same for the force response, predicting models with only temperature and temperature squared, indicating that while honing the processing method creates samples with a more repeatable response, the general trend remains the same. For the measure of stress relaxation represented by the F_d, no model showed statistical significance, indicating that the amount of stress relaxation remains the same for all tested processing methods after the process became more refined. In other words, F_d is not statistically different for any of the tested processing methods.

As predicted due to the change in testing procedure, the several samples above 190 °C proved to be influential outliers, as observed in the case-influence statistics. Once these data sets were removed, the influential variables in the predicted model for $F_{\max}$ remained nearly the same. The change was less influence of temperature squared. F_d again did not yield any model that predicts the behavior.

The empirical model for $F_{\max}$ for the refined data set and with samples 190 °C and under, with the accompanying statistical data, is (temperatures in Celsius):

Predicted Models:

$$F_{\max} = 0.128 + 0.004 * Temp + 1.10e - 5 * (Temp - 153)^2. \quad (2)$$

Lack-of-fit p-value: 0.038.

This model is shown over the all the data from the refined sample set in figure 6. The outliers above 190 °C are visible, the higher force response corresponding to the force required to break the adhesion.

It should be noted that the relative magnitude to the squared term is small when compared to the linear term. This term, in the expanded estimates shown in table 2, has the largest p-value showing the least statistical significance. Due to the spread in the data, a linear fit is a more accurate model

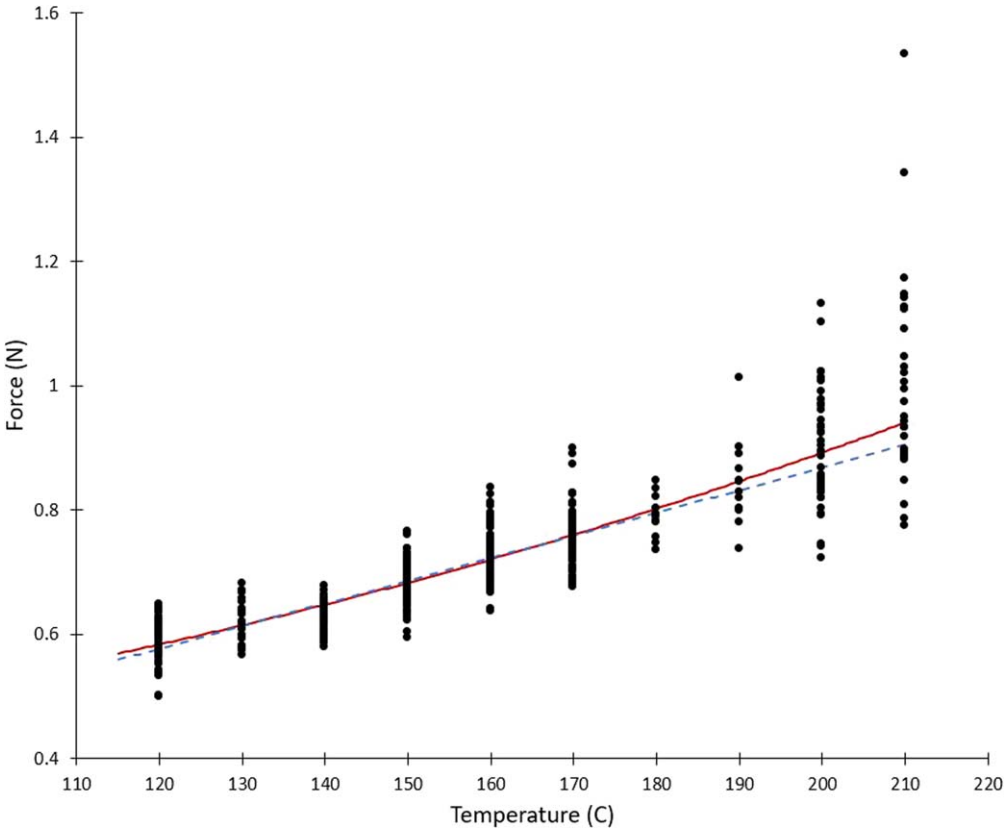

Figure 6. F_{max} versus temperature with the predicted models shown over the refined sample set. The solid (red) line is the model with temperature squared term. The dashed (blue) line is the linear model.

Table 2. Expanded estimates for equation (2).

Term	Estimate	Standard error	*t*-ratio	*p*-value	Lower 95% CL	Upper 95% CL
Intercept	0.128	0.019	6.67	<0.001	0.091	0.166
Temp	0.004	0.000 1	30.4	<0.001	0.004	0.004
$(\text{Temp-153})^2$	1.10×10^{-5}	5.57×10^{-6}	1.98	0.048	8.54×10^{-8}	2.20×10^{-5}

Table 3. Expanded estimates for equation (3).

Term	Estimate	Standard error	*t*-ratio	*p*-value	Lower 95% CL	Upper 95% CL
Intercept	0.141	0.018	7.71	<0.001	0.105	0.177
Temp	0.004	0.0001	30.7	<0.001	0.003	0.004

Table 4. Expanded estimates for equation (4).

Term	Estimate	Standard error	*t*-ratio	*p*-value	Lower 95% CL	Upper 95% CL
Intercept	0.994	0.021	47.6	<0.001	0.953	1.04
ln(3)	0.142	0.010	14.5	<0.001	0.122	0.161

to describe the trend. The resulting linear trend is (expanded estimates shown in table 3):

$$F_{max} = 0.141 + 0.004 * Temp. \quad (3)$$

Lack of fit *p*-value: 0.0158.

The force drop was an average of 0.123 N with a standard deviation of 0.043 N for the complete data set. For the refined set, the average was 0.121 N with a standard deviation of 0.055 N. The ratio of the average force drop over force max per sample batch was analyzed. There was no significant model that matched this, leading to the conclusion that the ratio is statistically unaffected by sampling method for the methods tested. The average ratio of F_d/F_{max} is 0.156 with a standard deviation of 0.017.

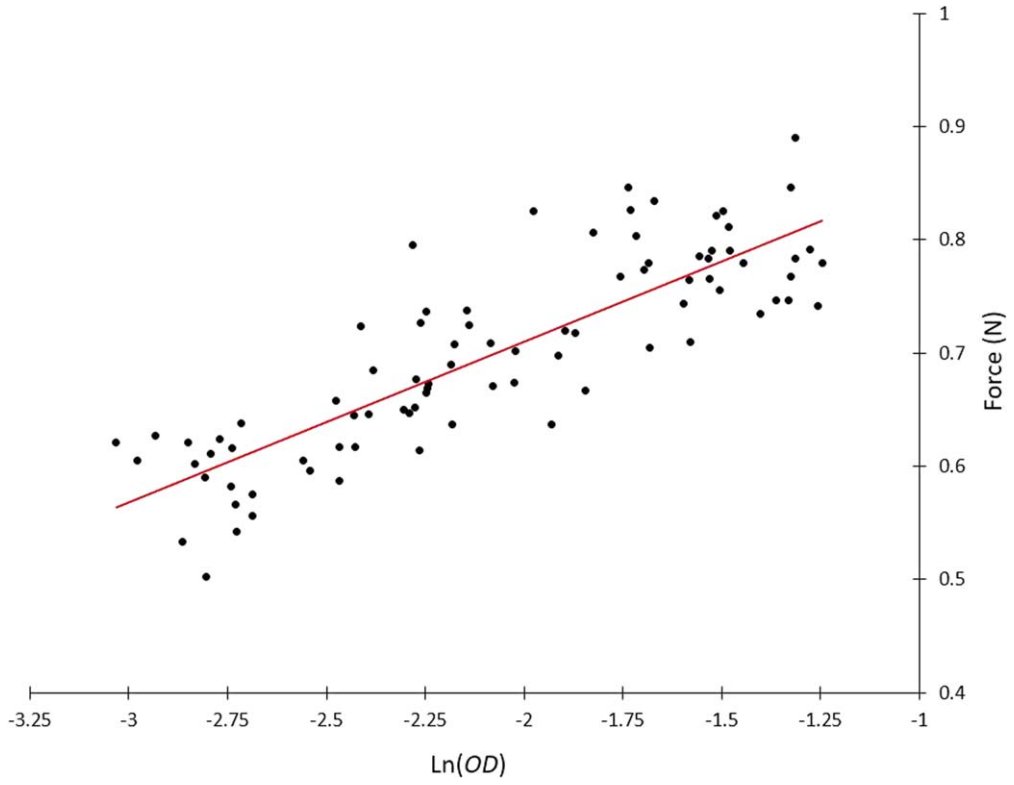

Figure 7. F_{max} versus ln(OD) with the predicted linear model shown.

Statistical analysis of the light absorption results with all samples resulted in a model containing temperature, temperature squared, and time. Once again, the temperatures above 190 °C proved to be the most influential to the model, although within the expected range. When removed, the model remained the same while the R^2 value increased. This model correlates well with the previous model, indicating the crystallinity increases in a similar manner to the force response of the crease. When comparing crystallinity directly to F_{max}, the data (using values under 190 °C and only repeated tests) pointed towards a logarithmic transformation of the optical density data. Once transformed, the model appeared to follow a roughly linear increase in F_{max} with increase in the natural logarithm of OD as seen in figure 7. Although the lack-of-fit p-value indicates only very little statistical significance, $p = 0.138$, the p-values of the individual estimates of the model are all highly significant. This indicates that there is likely be a relation of increasing crystallinity leading to higher force responses, and crystallinity likely plays a role in the force response of the PET origami sheets.

The predicted linear model (expanded estimates shown in table 4):

$$F_{max} = 0.99 + 0.14 * \ln(\text{OD}). \quad (4)$$

Lack-of-fit p-value: 0.138.

4. Discussion

After heat treatment, all samples remained in the fully folded configuration, verifying that using a heat treatment changes the natural position of origami patterns in the z-fold samples. During actuation, fold and facets both contributed to the total deflection. This was a result of the flexibility of the thin sheets used and the increased stiffness of the crease. The large amount of deflection chosen for the test was to ensure that some folding and unfolding was happening at the creases but did induce some plastic deformation of the creases themselves. As this work primarily focused around understanding the trends in heat setting and their overall effect on origami models, the conclusions are unaffected as clear trends were discovered in the effect of heat treatment on PET sheets.

Further work in the effects of individual heat treatments on PET sheets would likely include quantifying the amount of force a specific heat treatment can induce on a crease. This could be done using a moment-angle relationship and understanding these effects on a per unit length basis could help quantify the influence of a specific heat treatment on fold patterns and modeling the force to actuate entire patterns.

Differently sourced materials may contain different material properties, but the ability to change the natural position of a folded sample and alter the crystalline structure to increase the force response through annealing should remain the same. The trends of the effect on varying thicknesses and geometries should also be the same. Future work could study the specific effects of variations in material and geometry. In PET, the temperature of annealing was found to be highly influential on the performance of the origami sample. There appears to be an approximately linear increase of force response with increases in annealing temperature. Future work could include investigating the ability to heat set

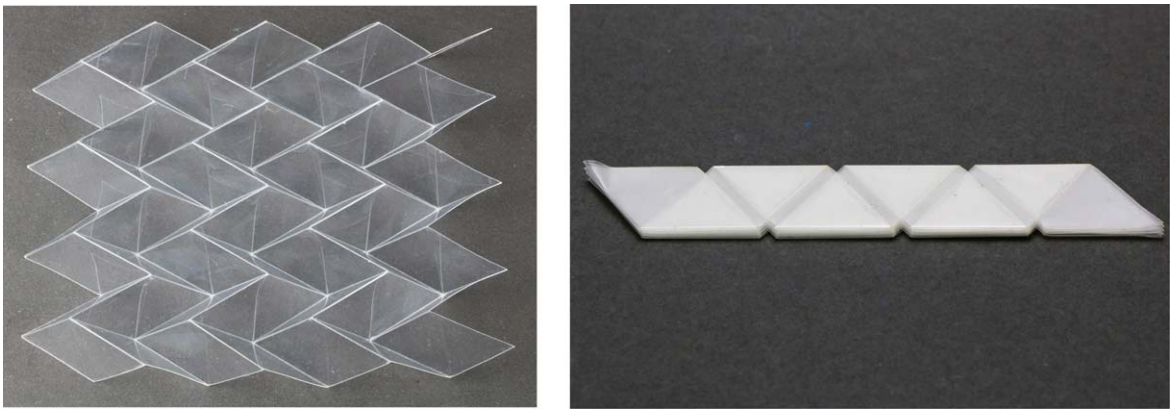

(a) Natural state after creasing and before heat set (b) Natural state after heat set

Figure 8. Miura-ori tessellation before (a) and after (b) heat setting treatment in completely folded configuration. (a) Natural state after creasing and before heat set, (b) natural state after heat set.

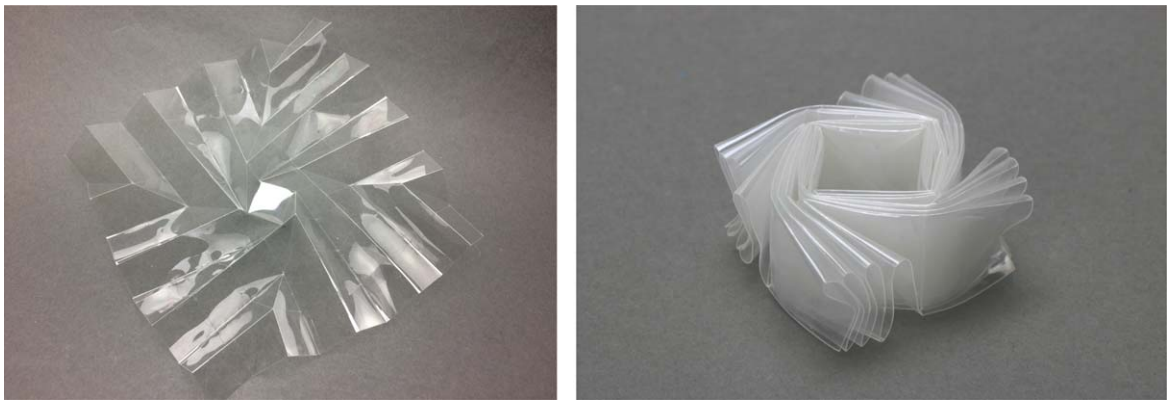

(a) Natural state after creasing and before heat set (b) Natural state after heat set

Figure 9. A Flasher pattern before (a) and after (b) heat setting treatment. (a) Natural state after creasing and before heat set. (b) Natural state after heat set.

other polymer sheets and the trends in heat setting parameters for those polymers.

For PET origami design, due to the difficulty of placing a barrier between every panel of a complex model during manufacture, temperatures above 190 °C are not recommended for use. Optimal results for usability were obtained in temperatures from 160 °C–180 °C. No significant difference was observed in the two cooling methods. Physical validation of the processing on more complex patterns were performed using a processing method with an annealing temperature of 170 °C, a temperature in the middle of the optimal range and the highest temperature where no adhesion was observed. Given that for the times analyzed there was no statistical difference in the crease response, a 60 min annealing time was used to conserve time and energy costs. The Drop Cooling decreases time required to cool the model and is recommended for use.

The influence of tightly controlling the temperature of heating showed a reduction in the spread in the results. Through the repetition the earlier batches, it was shown that the average result is repeatable and that careful consideration in the control of annealing temperature plays an influential role in the precision of results.

To summarize the recommended processing methods resulting from this work, an annealing time of at least 60 min at 160 °C–180 °C with a Drop Cooling method results in the strongest force response in the crease while avoiding panel adhesion. For physical validation in the more complex origami models, 60 min at 170 °C with Drop Cooling was used.

4.1. Miura-ori tessellation

The Miura-ori was chosen because it is a basic tessellation with diverse applications [21, 42–46] and its elements appear in many other patterns (figure 8). It is also rigid-foldable, meaning strain only occurs in the creases. Two samples were made with one treated in a completely folded configuration (figure 8(b)) and the other in an intermediate folded state to show that the treatment can apply to intermediate fold positions. Both samples showed similar responses as the previous patterns with high bias to the heat set position.

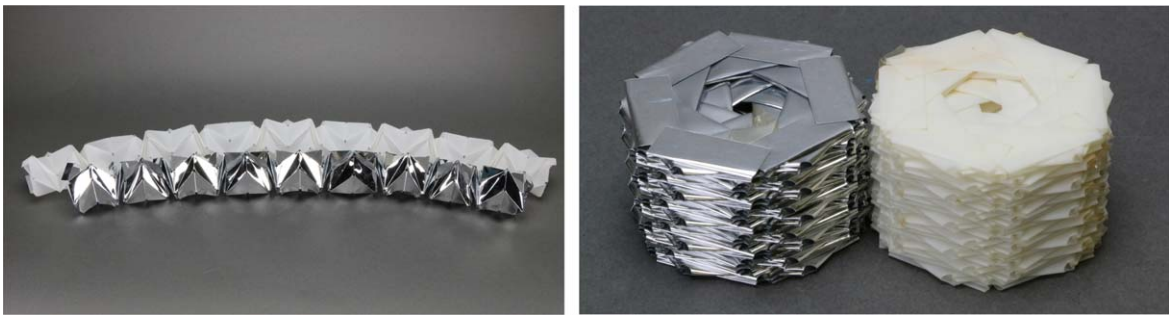

(a) Natural state after creasing and before heat set (b) Natural state after heat set

Figure 10. A modified triangulated cylinder tessellation before (a) and after (b) heat setting treatment. (a) Natural state after creasing and before heat set. (b) Natural state after heat set.

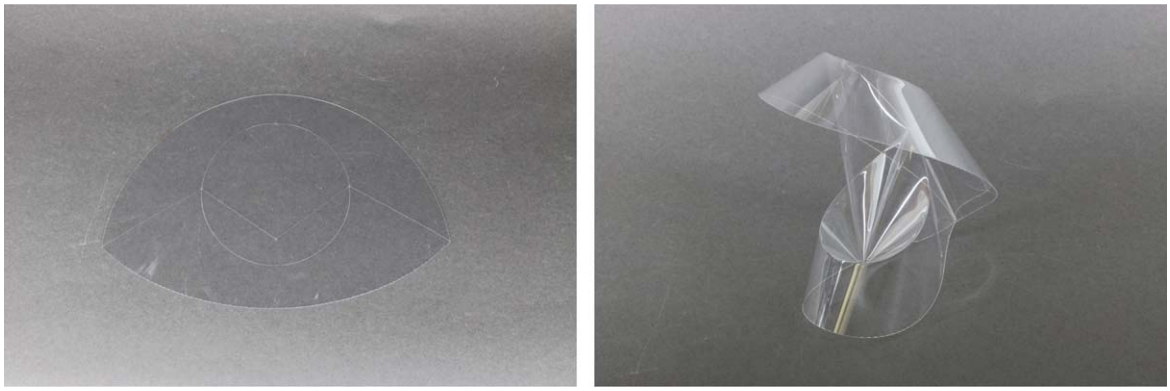

(a) Natural state before creasing and heat set (b) Natural state after heat set

Figure 11. An Elliptic Infinity before (a) and after (b) heat setting treatment. (a) Natural state before creasing and heat set, (b) Natural state after heat set.

4.2. Flasher pattern

The flasher pattern was chosen due to the complexity of its deployed-to-stowed actuation. This pattern has been proposed for use in space solar arrays [47, 48]. When folded in PET, the pattern tends toward the deployed position (figure 9(a)). The goal of the heat set was to evaluate whether the complex pattern would favor the stowed configuration. The pattern was scored, folded, restrained, and then heat set in the folded state. After processing, the pattern remained in the stowed state after the restraints were removed (figure 9(b)). The pattern actuated smoothly to the extended state and returned to the folded position.

4.3. Modified triangulated cylinder tessellation

Recent work has investigated the use of a modified triangulated cylinder origami tessellation in many applications [26, 52–55]. This particular pattern is not rigid-foldable, meaning that strain is induced in the creases and panels during actuation. This behavior increases the tendency of the model to return to its initial folded configuration. This can be advantageous if the design application requires axial stiffness. Stress relaxation also becomes important if the pattern is designed to be used in an application where it is stretched away from the natural length for long periods of time.

Implementing the process method discussed, it was shown that the natural length of the pattern could be changed from the extended position inherent in the manufacturing method to a fully-compressed state. One of the test models before heat treating is shown in figure 10(a). The same model after treatment is shown in figure 10(b). The pattern showed a strong bias to the heat set position and held the majority of the bias even when stretched to the pre-treatment configuration for over a hour. For these models, one PET sheet was metalized on one side and the other PET sheet contained a color agent giving it a matte white appearance. These changes in material were selected to see if the treatment would still be effective in various types of available PET products. Both responded as expected with no observable difference after heat treatment.

4.4. Elliptic infinity pattern

The Elliptic Infinity developed by origami artist Robert Lang [50] was investigated to see the effect of the processing method on curved folds. This pattern consists of two large curved folds and four straight folds, as shown in figure 11(a). Before heat treatment, adhesive is required to constrain the pattern in the folded state. After applying the heat treatment, the adhesive was removed and the pattern did not move from the folded configuration (figure 11(b)). The pattern

consistently returned to the folded position after deflection with the exception of fold lines which experience kinematic change points during folding. These results show the treatment to be effective on curve folds.

4.5. Potential applications

Through the processing of the PET strips and origami patterns, we have shown that the polymer can be configured to have a preferred position to which it will return after actuation. This has multiple applications. One is in self-retracting mechanisms. When treated in the stowed state, as in the case of the triangulated cylinder and flasher pattern examples, the pattern can be extended to perform a function and then automatically retracted to a stowed position for storage or transport. This bias towards the stowed position can also add tension into the pattern, which can be used to add stability to the mechanism through pre-tensioning. The added tension between the supports used to actuate the mechanism increases the stiffness. This can also be applied if the mechanism is designed to be in the deployed state for an extended period of time. The tension assists in making the pattern act more like a structure, such as in a tensegrity structure where tension makes flexible members behave as rigid links.

This processing also has application in self-deploying mechanisms. The need for self-deploying mechanisms is common in many areas, including deployment of medical devices designed to enter the body in a compact configuration and deploy for use in the body, and space systems that are compact for launch and self-deploy to reduce the need for external actuators. By processing the pattern into a folded or semi-folded state, it can be laid flat for storage or insertion and self-deploy to the desired state when the pressure is released.

5. Conclusion

The stiffness of the fold in PET sheets has been shown to be tailorable through heat processing. This can be applied to many origami patterns and origami engineering applications. Therefore, PET can be tailored to the specific application desired. The treatment processes considered can provide a framework for determining the optimal process parameters for a given application.

All processing methods test data used in this study has been made available through Brigham Young University's ScholarsArchive, an open-access online data storage site. The raw data from each sample test is included, as well as comprehensive reviews of all data sets collectively which were used in the statistical analysis. These files can be accesses at https://scholarsarchive.byu.edu/data/.

Of the processing methods considered, temperature of processing was determined to be the primary factor in determining the force response. This relationship was found to be approximately linear. Models heated well above the cold-crystallization temperature had a larger force response when stretched than those heated below T_c. Crystallinity appears to have a relation in the crease properties of PET sheet with higher crystallinities resulting in higher force responses. The stress relaxation in the fold was insensitive to the processing methods considered. Understanding these trends in heat setting and its effect on PET sheets can provide the initial framework for future work in creating polymer-based origami engineering designed and tailored to specific needs and application.

Acknowledgments

Special thanks to Jared Butler, Kenny Seymour, Makenna Foulkrod, and Mary Wilson for help in cutting and folding the test samples and helping with physical validation. This paper is based on work supported by the U.S. National Science Foundation and the US Air Force Office of Scientific Research through NSF Grant No. EFRIODISSEI-1240417, by NSF Grant No. 1663345, and by Intuitive Surgical, Inc.

ORCID iDs

Brandon Sargent https://orcid.org/0000-0002-7997-4494
William G Pitt https://orcid.org/0000-0002-6043-3452
Larry L Howell https://orcid.org/0000-0001-8132-8822

References

[1] Turner N, Goodwine B and Sen M 2016 A review of origami applications in mechanical engineering *Proc. Inst. Mech. Eng.* C **230** 2345–62
[2] Morgan J, Magleby S P and Howell L L 2016 An approach to designing origami-adapted aerospace mechanisms *J. Mech. Des.* **138** 052301
[3] Thrall A and Quaglia C 2014 Accordion shelters: a historical review of origami-like deployable shelters developed by the us military *Eng. Struct.* **59** 686–92
[4] Lang R J 2017 *Twists, Tilings, and Tessellations: Mathematical Methods for Geometric Origami* (Boca Raton, FL: AK Peters/CRC Press)
[5] Dudte L H, Vouga E, Tachi T and Mahadevan L 2016 Programming curvature using origami tessellations *Nat. Mater.* **15** 583
[6] Tachi T 2013 Designing freeform origami tessellations by generalizing resch's patterns *J. Mech. Des.* **135** 111006
[7] Lv C, Krishnaraju D, Konjevod G, Yu H and Jiang H 2014 Origami based mechanical metamaterials *Sci. Rep.* **4** 5979
[8] Howell L L 2018 Complex mechanical motion guided without external control *Nature* **561** 470–1
[9] Hanna B H, Lund J M, Lang R J, Magleby S P and Howell L L 2014 Waterbomb base: a symmetric single-vertex bistable origami mechanism *Smart Mater. Struct.* **23** 094009
[10] Johnson M, Chen Y, Hovet S, Xu S, Wood B, Ren H, Tokuda J and Tse Z T H 2017 Fabricating biomedical origami: a state-of-the-art review *Int. J. Comput. Assist. Radiol. Surg.* **12** 2023–32

[11] Kshad M A E, Popinigis C and Naguib H E 2018 3D printing of ron-resch-like origami cores for compression and impact load damping *Smart Mater. Struct.* **28** 015027
[12] Morgan J, Magleby S P and Howell L L 2016 An approach to designing origami-adapted aerospace mechanisms *J. Mech. Des.* **138** 052301
[13] Mailen R, Wagner C H, Bang R S, Zikry M, Dickey M D and Genzer J 2019 Thermo-mechanical transformation of shape memory polymers from initially flat discs to bowls and saddles *Smart Mater. Struct.* **28** 045011
[14] Mailen R W, Dickey M D, Genzer J and Zikry M 2017 Effects of thermo-mechanical behavior and hinge geometry on folding response of shape memory polymer sheets *J. Appl. Phys.* **122** 195103
[15] Deng D, Yang Y, Chen Y, Lan X and Tice J 2017 Accurately controlled sequential self-folding structures by polystyrene film *Smart Mater. Struct.* **26** 085040
[16] Miyashita S, Guitron S, Li S and Rus D 2017 Robotic metamorphosis by origami exoskeletons *Sci. Robot.* **2** eaao4369
[17] Peraza-Hernandez E A, Hartl D J, Malak R J Jr and Lagoudas D C 2014 Origami-inspired active structures: a synthesis and review *Smart Mater. Struct.* **23** 094001
[18] Felton S, Tolley M, Demaine E, Rus D and Wood R 2014 A method for building self-folding machines *Science* **345** 644–6
[19] Ahmed S, Ounaies Z and Frecker M 2014 Investigating the performance and properties of dielectric elastomer actuators as a potential means to actuate origami structures *Smart Mater. Struct.* **23** 094003
[20] Akbari S, Sakhaei A H, Kowsari K, Yang B, Serjouei A, Yuanfang Z and Ge Q 2018 Enhanced multimaterial 4D printing with active hinges *Smart Mater. Struct.* **27** 065027
[21] Muhs F, Klett Y and Middendorf P 2018 Automated numerical process chain for the design of folded sandwich cores *Proc. 7th Int. Meeting on Origami in Science, Mathematics and Education (7OSME)*
[22] Klett Y 2018 Paleo: Plastically annealed lamina emergent origami *ASME 2018 International Design Engineering Technical Conferences and Computers and Information in Engineering Conference* (American Society of Mechanical Engineers) p V05BT07A062
[23] Sareh P, Chermprayong P, Emmanuelli M, Nadeem H and Kovac M 2018 Rotorigami: a rotary origami protective system for robotic rotorcraft *Sci. Robot.* **3** eaah5228
[24] Glugla D J, Alim M D, Byars K D, Nair D P, Bowman C N, Maute K K and McLeod R R 2016 Rigid origami via optical programming and deferred self-folding of a two-stage photopolymer *ACS Appl. Mater. Interfaces* **8** 29658–67
[25] Seymour K, Burrow D, Avila A, Bateman T, Morgan D C, Magleby S P and Howell L L 2018 Origami-based deployable ballistic barrier *Proc. 7th Int. Meeting on Origami in Science, Mathematics and Education (7OSME)*
[26] Butler J, Morgan J, Pehrson N, Tolman K, Bateman T, Magleby S P and Howell L L 2016 Highly compressible origami bellows for harsh environments *ASME 2016 Int. Design Engineering Technical Conf. and Computers and Information in Engineering Conf.* (https://doi.org/10.1115/DETC2016-59060)
[27] Lang R J, Tolman K A, Crampton E B, Magleby S P and Howell L L 2018 A review of thickness-accommodation techniques in origami-inspired engineering *Appl. Mech. Rev.* **70** 010805
[28] Tachi T 2011 Rigid-foldable thick origami *Origami* **5** 253–64
[29] Chen Y, Peng R and You Z 2015 Origami of thick panels *Science* **349** 396–400
[30] Ma W *et al* 2018 An origami-inspired cube pipe structure with bistable anti-symmetric cfrp shells driven by magnetic field *Smart Mater. Struct.* **28** 025028
[31] Wu R, Roberts P C, Lyu S, Soutis C, Zheng F, Diver C, Gresil M and Blaker J J 2018 Rigidisation of deployable space polymer membranes by heat-activated self-folding *Smart Mater. Struct.* **27** 105037
[32] Chen N, Liu C Y and Stringer J 2019 Autonomous origami: pre-programmed folding of inkjet printed structures *Smart Mater. Struct.* **28** 055019
[33] Flores A, Pieruccini M, Nöchel U, Stribeck N and Calleja F B 2008 Recrystallization studies on isotropic cold-crystallized PET: influence of heating rate *Polymer* **49** 965–73
[34] Cho D H, Yu W-R, Youk J H and Yoo J H 2007 Formation of micro-crystals in poly (ethylene terephthalate) fiber by a short heat treatment and their influence on the mechanical properties *Eur. Polym. J.* **43** 3562–72
[35] Fakirov S 2008 *Oriented Polymer Materials* (New York: Wiley)
[36] Balani K, Verma V, Agarwal A and Narayan R 2015 *A Materials Science and Engineering Perspective* (Hoboken, NJ: John Wiley & Sons, Inc.)
[37] Chen W, Lofgren E and Jabarin S 1998 Microstructure of amorphous and crystalline poly (ethylene terephthalate) *J. Appl. Polym. Sci.* **70** 1965–76
[38] Karagiannidis P G, Stergiou A C and Karayannidis G P 2008 Study of crystallinity and thermomechanical analysis of annealed poly (ethylene terephthalate) films *Eur. Polym. J.* **44** 1475–86
[39] Abou-Kandil A I and Windle A H 2007 The development of microstructure in oriented polyethylene terephthalate (PET) during annealing *Polymer* **48** 5069–79
[40] Martins C I and Cakmak M 2007 Control the strain-induced crystallization of polyethylene terephthalate by temporally varying deformation rates: a mechano-optical study *Polymer* **48** 2109–23
[41] Suzuki A and Mochiduki N 2001 Mechanical properties and superstructure of poly (ethylene terephthalate) fibers zone-drawn and zone-annealed by CO_2 laser heating *J. Appl. Polym. Sci.* **82** 2775–83
[42] Cui J, Adams J G and Zhu Y 2018 Controlled bending and folding of a bilayer structure consisting of a thin stiff film and a heat shrinkable polymer sheet *Smart Mater. Struct.* **27** 055009
[43] Tolman S S, Delimont I L, Howell L L and Fullwood D T 2014 Material selection for elastic energy absorption in origami-inspired compliant corrugations *Smart Mater. Struct.* **23** 094010
[44] Miura K 2009 The science of miura-ori: a review *4th International Meeting of Origami Science, Mathematics, and Education* ed R J Lang (Natick, MA: AK Peters) pp 87–100
[45] Cheung K C, Tachi T, Calisch S and Miura K 2014 Origami interleaved tube cellular materials *Smart Mater. Struct.* **23** 094012
[46] Sane H, Bhovad P and Li S 2018 Actuation performance of fluidic origami cellular structure: a holistic investigation *Smart Mater. Struct.* **27** 115014
[47] Pehrson N A, Smith S P, Ames D C, Magleby S P and Arya M 2019 Self-deployable, self-stiffening, and retractable origami-based arrays for spacecraft *AIAA Scitech 2019 Forum* p 0484
[48] Zirbel S A, Lang R J, Thomson M W, Sigel D A, Walkemeyer P E, Trease B P, Magleby S P and Howell L L 2013 Accommodating thickness in origami-based deployable arrays *J. Mech. Des.* **135** 111005
[49] Guest S D and Pellegrino S 1994 The folding of triangulated cylinders:I. Geometric considerations *J. Appl. Mech.* **61** 773–7
[50] Lang R J 2013 One ellipse to rule them all (https://origamiusa.org/thefold/article/) one-ellipse-rule-them-all

[51] Nelson T G, Lang R J, Pehrson N A, Magleby S P and Howell L L 2016 Facilitating deployable mechanisms and structures via developable lamina emergent arrays *J. Mech. Robot.* **8** 031006

[52] Filipov E T, Tachi T and Paulino G H 2015 Origami tubes assembled into stiff, yet reconfigurable structures and metamaterials *Proc. Natl Acad. Sci.* **112** 12321–6

[53] Cai J, Deng X, Zhou Y, Feng J and Tu Y 2015 Bistable behavior of the cylindrical origami structure with Kresling pattern *J. Mech. Des.* **137** 061406

[54] Kresling B, Abel J F and Cooke Robert J 2008 Natural twist buckling in shells: from the Hawkmoth's bellows to the deployable Kresling-pattern and cylindrical Miura-Ori *Proc. 6th Int. Conf. on Computation of Shell and Spatial Structures (Ithaca)* ed J F Abel and J Robert Cooke

[55] Butler J, Magleby S, Howell L, Mancini S and Parness A 2017 Highly compressible origami bellows for microgravity drilling-debris containment *AIAA SPACE and Astronautics Forum and Exposition* p 5341